Electronic Supplementary Material (ESI) for Inorganic Chemistry Frontiers.

Neutral Cobalt(II)-Bis(Benzimidazole)Pyridine Field-Induced Single-Ion Magnets for Surface Deposition

Jana Juráková,[a] Ondrej F. Fellner,[b] Sören Schlittenhardt,[c] Šárka Vavrečková,[a] Ivan Nemec,[a,b] Radovan Herchel,[b] Erik Čižmár,[d] Vinicius Tadeu Santana,[a] Milan Orlita,[e] Denis Gentili,[f] Giampiero Ruani,[f] Massimiliano Cavallini,[f] Petr Neugebauer,[a] Mario Ruben,[c] Ivan Šalitroš[ag*]

a) Central European Institute of Technology, Brno University of Technology, Purkyňova 123, 61200 Brno Czech Republic
b) Department of Inorganic Chemistry, Faculty of Science, Palacký University, 17. listopadu 12, 771 46 Olomouc, Czech Republic
c) Institute of Nanotechnology (INT), Karlsruhe Institute of Technology (KIT), Hermann-von-Helmholtz-Platz 1, 76344 Eggenstein-Leopoldshafen (Germany).
d) Institute of Physics, Faculty of Science, P.J. Šafárik University Park Angelinum 9, 04154 Košice, Slovakia
e) LNCMI-EMFL, CNRS UPR3228, Univ. Grenoble Alpes, Univ. Toulouse, Univ. Toulouse 3, INSA-T, Grenoble and Toulouse, France
f) Consiglio Nazionale delle Ricerche, Istituto per lo Studio dei Materiali Nanostrutturati (CNR-ISMN), Via P. Gobetti 101, 40129 Bologna, Italy
g) Department of Inorganic Chemistry, Faculty of Chemical and Food Technology, Slovak University of Technology in Bratislava. Bratislava SK-81237, Slovakia. *e-mail: ivan.salitros@stuba.sk

S1 Experimental section

Materials and methods

The synthesis of ligands L1 (2,6-bis(1-octyl-1*H*-benzimidazol-2-yl)pyridine) and L2 (2,6-bis(1-dodecyl-1*H*-benzimidazol-2-yl)pyridine) was reported previously.[1] Acetonitrile p.a., and $Co(NO_3)_2 \cdot 6H_2O$ were purchased from Sigma-Aldrich or Mikrochem and used as received without any further purification. IR spectra in the interval from 4000 to 400 cm^{-1} of herein reported compounds were measured on Nicolet 5700 spectrometer (ATR technique). Elemental analysis of carbon, hydrogen and nitrogen was carried out by EA CHNS(O) Flash 1112 machine The UV-VIS spectra were measured in solid state on Specord 200 spectrophotometer in the range of 800 – 200 nm.

Synthesis

Synthesis of complexes **1** [Co(L1)$(NO_3)_2$] and **2** [Co(L2)$(NO_3)_2$]

$Co(NO_3)_2 \cdot 6H_2O$ (146 mg, 0.5 mmol, 1 eq) was dissolved in 10 ml of acetonitrile and added into the acetonitrile solution (30 ml) of ligand **L1** (268 mg, 0.5 mmol, 1 eq) or **L2** (324 mg, 0.5 mmol, 1 eq), respectively. When Co(II) salt was added, the color change from pale yellow to orange occurred immediately without the formation of precipitation. Reaction mixture was refluxed for 4 hours, filtered and mother liquor was submitted to the controlled evaporation at room temperature in order to grow single crystals suitable for the diffraction analysis. The orange crystals of **1** were collected by filtration after few days.

Complex **1 [Co(L1)$(NO_3)_2$]**: Yield 41% (151 mg, 0.21 mmol). Elemental analysis for $C_{35}H_{45}CoN_7O_6$ (M_w = 718.71 g mol^{-1}) found % (expected %): C 58.19 (58.49); N 13.84 (13.64); H 6.32 (6.31). FT−IR (ATR, $\tilde{\nu}_{max}/cm^{-1}$): 2922, 2854 (m, $\nu(C_{al}\text{-}H)$); 1598, 1574 (m, $\nu(C_{ar}\text{-}C_{ar})$ or $\nu(CN)$); 748 (s, $\delta(CH)$). UV-VIS (nujol, λ/nm): 290 - 410 (π→π*, n→π*, 500 - 575 (MLCT and/or d-d). UV-VIS (acetonitrile, λ/nm): 290 (π→π*), 375 (n→π*).

Complex **2 [Co(L2)$(NO_3)_2$]**: Yield 38% (158 mg, 0.19 mmol). Elemental analysis for $C_{43}H_{61}CoN_7O_6$ (M_w = 830.91g mol^{-1}) found % (expected %): C 62.13 (62.16); N 12.32 (11.80); H 7.42 (7.40). FT−IR (ATR, $\tilde{\nu}_{max}/cm^{-1}$): 2918, 2850 (m, $\nu(C_{al}\text{-}H)$); 1599, 1573 (m, $\nu(C_{ar}\text{-}C_{ar})$ or $\nu(CN)$); 748 (s, $\delta(CH)$). UV-VIS (nujol, λ/nm): 290 - 410 (π→π*, n→π*, 500 - 575 (MLCT and/or d-d). UV-VIS (acetonitrile, λ/nm): 290 (π→π*), 375 (n→π*).

Surface depositions and characterisation

Drop casting: Films of **1** and **2** were grown by drop casting 10 µl of 1 g/L solution in chloroform (Sigma Aldrich anhydrous, 99.8%) in air. The substrates were of 10x10 mm^2 pieces of silicon covered by 200 nm of SiO_2. They were cleaned by sonication in acetone, in 2-propanol, and then dried under a stream of nitrogen.

Patterning: Patterning was performed by the lithographically controlled wetting. The protocol is reported in ref. 20a of the text. PDMS stamp is placed on a thin film of solution casted on the silicon surface. The capillary action pins the solution under the stamp protrusions leaving the other space free of solution in air. As the solution shrink, the solute precipitates onto the substrate within the menisci, producing the printed structures. Figure S1 shows the scheme of the process.

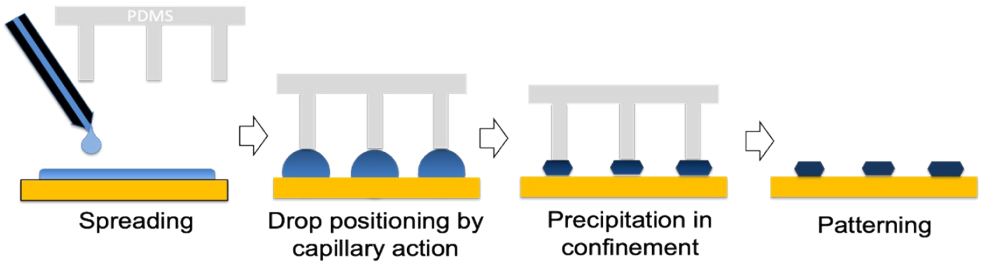

Figure S1 Scheme of lithographically controlled wetting

The stamps were made of poly-dimethylsiloxane, (Sylgard 184 by Dow Corning). They were prepared by replica moulding and curing for 6 h at 70°C, of a blank compact disk made of parallel lines.[2]

Optical microscopy: Optical images were recorded with a Nikon i-80 microscope equipped with crossed polarizers. The images were recorded using a commercial CCD camera (Nikon CCD DS-2Mv).

Atomic Force Microscopy: Scanning probe microscopy characterizations were performed on a Multimode 8 microscope equipped with a Nanoscope V controller and type J piezoelectric scanner (Bruker, USA). Samples were scanned at 0.5 Hz/line in PeakForce mode using Scanasyst-Air probes (Bruker, USA) in air, imposing an applied force of 2.5 nN.

Raman spectroscopy: Raman spectra were recorded at room temperature in back-scattering geometry using a Renishaw 1000 micro-Raman, exciting at 632.8 nm and collecting the scattered light for 800 sec each focusing on the sample through a x100 objective. To avoid local heating of the crystals, laser power was kept at 0.1 mW although no heating effects were observed even at higher power.

Sublimation: A home-built high-vacuum sublimation chamber equipped with a quartz crucible was used to test the sublimation of reported compounds. Sublimation chamber was heated by silicon nitride heater (BACH RC GmbH, Seefeld, Germany) with a thermocouple in thermal contact with the crucible. The base chamber pressure during the sublimation was 1×10^{-6} mbar. The compounds started to sublime above 270°C and 310°C.

XPS: X-ray photoelectron (XPS) measurements were carried out with a Kratos Axis Supra (Kratos Analytical, Manchester, United Kingdom) spectrometer at room temperature and under ultra-high vacuum (UHV) conditions. The instrument was equipped with a monochromatic Al Kα source of 1486.6 eV (15 mA, 15 kV) and a hemispherical analyser with a hybrid magnetic and electrostatic lens for enhanced electron collection. Survey and detailed XPS spectra were acquired at normal emission with fixed pass energies of 160 and 20 eV, respectively. All spectra were calibrated to the hydrocarbon peak set to 284.8 eV. The Kratos charge neutralizer system was used on all specimens. The inelastic backgrounds in all the spectra were subtracted according to the Shirley method.[3] Data analysis was based on a standard deconvolution method using a mixed Gaussian (G) and Lorentzian (L) line shape (G = 70% and L = 30%, Gaussian–Lorentzian product) for each component in the spectra. The spectra were analyzed using the CasaXPS software (version 2.3.18).

Diffraction experiments

The single-crystal diffraction data for **1** and **2** were collected at two different temperatures (**1HT** at 298 K and **1LT** 100 K, **2HT** at 298 K and **2LT** at 90 K) using an XtaLAB Synergy-I diffractometer with a HyPix3000 hybrid pixel array detector and microfocused PhotonJet-I X-ray source (Cu Kα). The absorption corrections were applied using the program CrysAlisPro 1.171.40.82a.[4] The structure was solved using SHELXT[5] program and refined by the full matrix least-squares procedure with SHELX[6] in OLEX2 (version 1.5).[7] All non-hydrogen atoms were refined anisotropically. All hydrogen atoms were found from the Fourier difference map and refined using the "riding" model. Non-routine aspects of crystal structure refinement: The crystals of **1HT** did not diffract well at room temperature, which allowed us to collect data in reasonable time only up to a maximal resolution of 0.89Å. In **1HT** the disordered of one aliphatic chain was modelled as disorder over two positions (ratio of occupation factors: 69:31). Same aliphatic chain is also disordered over two positions in **1LT** (ratio of occupation factors: 59:41). In **2HT**, the disorder of one aliphatic chain was modelled as disorder over two positions (ratio of occupation factors: 67:33).

Magnetic measurements

Herein reported magnetic investigation have been carried out on MPMS SQUID XL-5 and MPMS SQUID 3 (Quantum design Inc., San Diego, CA, USA). The exact amount of sample was mixed with melted eicosane and filled into the gelatine capsule, which has been used as the sample holder. In the case of magnetic experiments at static magnetic field (DC), the temperature-dependency was recorded in the thermal range 1.9 – 300 K at B = 0.1 T using the 1 K/min sweeping rate, and field-dependency was measured at isothermal conditions in the range B = 0 – 7 T. Collected data were corrected for the diamagnetism of eicosane and gelatine capsule as well as for the molecular diamagnetic contribution,

which was calculated using the Pascal constants.[8] Magnetic functions were transformed into the χT vs T and M_{mol} vs B dependencies. The experimental details about the magnetic experiments at AC magnetic field are given in the section S8 (*vide infra*).

HF EPR and FIRMS spectroscopy

High-frequency electron paramagnetic resonance (HFEPR) spectra were acquired using a custom-built spectrometer comprising a cryogen-free 16 T superconducting magnet (Cryogenics Ltd, London, UK), microwave sources (Virginia Diodes Inc., Charlottesville, VA, USA), and quasi-optical components (Thomas Keating Ltd, Billingshurst, UK).[9] Each compound was milled with 10% eicosane and then compressed into a 5 mm pellet that was subsequently positioned within a sample holder equipped with a modulation coil and temperature sensor. The sample holder, attached to a probe, was inserted into the magnet bore within a variable temperature insert (VTI) cryostat for temperature control. The HFEPR measurements were performed using a modulation frequency of 50 kHz and amplitude of 0.5 mT at different frequencies and temperatures as indicated within each figure.

Fourier-transform infrared magnetic spectroscopy (FIRMS) was employed to examine the magneto-optical response of the sample in the terahertz (THz) range. Measurements were conducted in the standard Faraday configuration, i.e., in transmission mode, with unpolarised light and the magnetic field parallel to the wave vector of the probing radiation. The compounds were combined with 90% eicosane and pressed into pellets to ensure transparency in this spectral range. The magneto-transmission was measured using radiation from a Hg arc lamp that was analysed using a Vertex 80v Fourier-transform spectrometer and delivered through light-pipe optics to the pellet situated inside a superconducting coil for sweeping magnetic field up to16 T, maintained in helium heat-exchange gas at T = 4.2 K. After passing through the pellet, the radiation was detected using a composite bolometer placed just below it. The FIRMS spectra were normalised by dividing them by the zero-field transmission spectrum, and at each magnetic field, by the spectrum from the previous magnetic field. We also employed the derivative of the spectra with respect to the energy to highlight the small features corresponding to the magnetic-dependent peaks, enabling to observe the shifts in magnetic field-dependent lines clearly. Simulations for HFEPR and FIRMS data were performed using EasySpin[10] in MATLAB.[11]

X-band EPR

The EPR spectra were studied using Bruker ELEXSYS II E500 X–band spectrometer (Bruker BioSpin GmbH, Rheinstetten, Germany) with an operating frequency of 9.4 GHz equipped with ESR910 helium flow–type cryostat (Oxford Instruments plc, Abingdon, UK). The powdered sample was mixed with Apiezon N grease (M&I Materials Ltd, Manchester, UK) and attached to the Suprasil quartz sample holder (Wilmad-LabGlass, Vineland, NJ, USA).

S2 Spectral characterization of prepared compounds

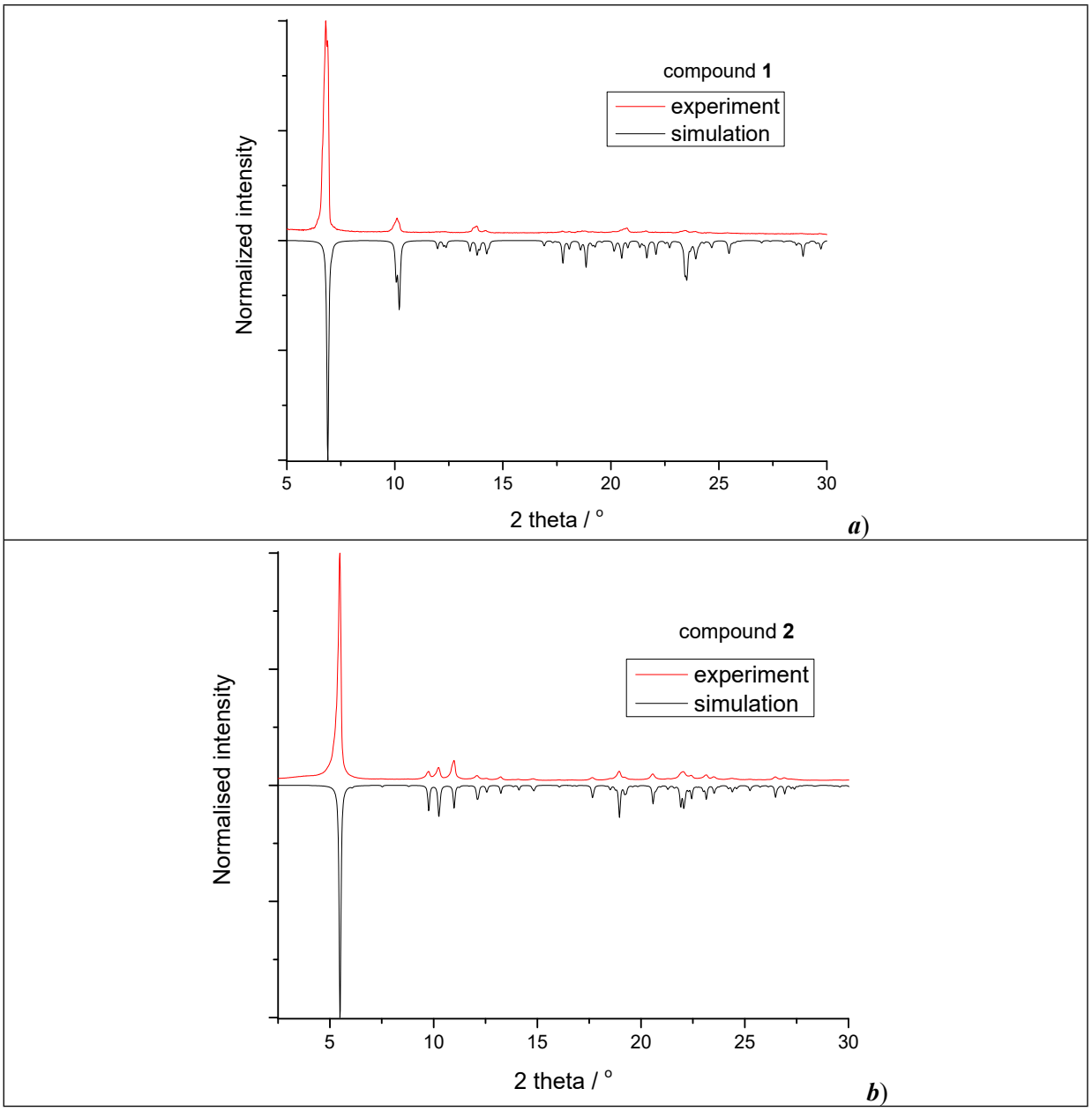

Figure S2 X-ray powder diffractogram of **1** (*a*) and **2** (*b*).

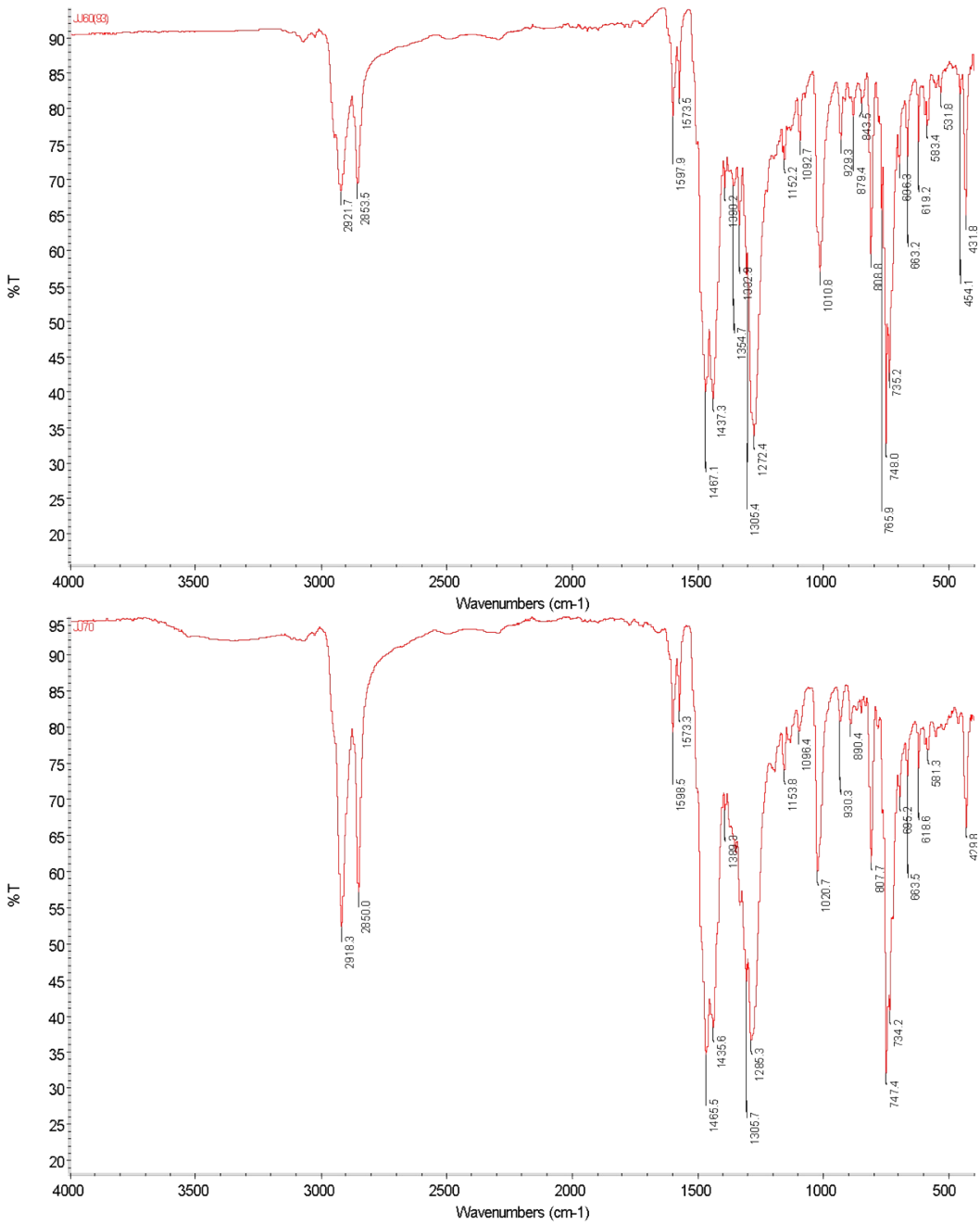

Figure S3 FT-IR spectra of **1** (*a*) and **2** (*b*).

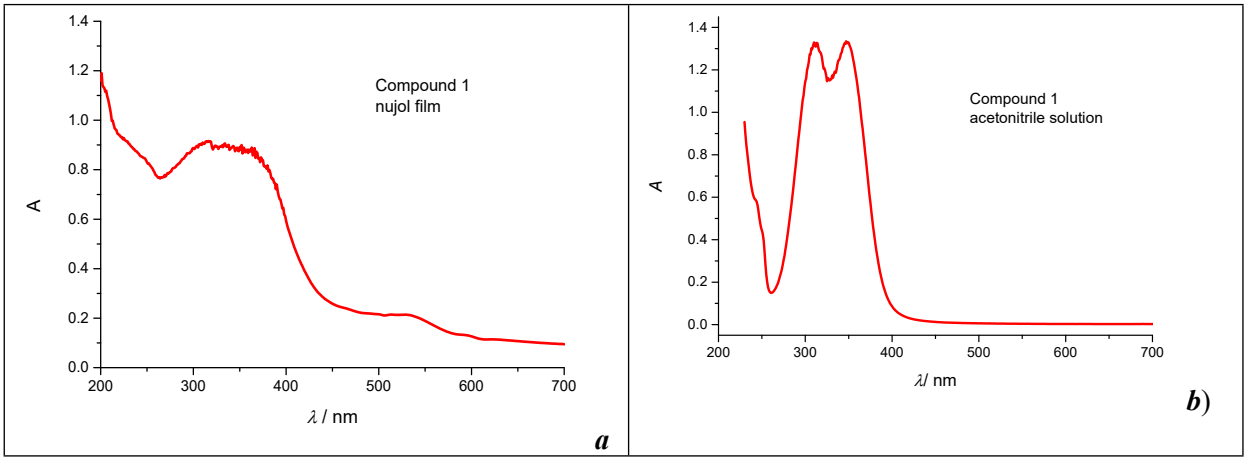

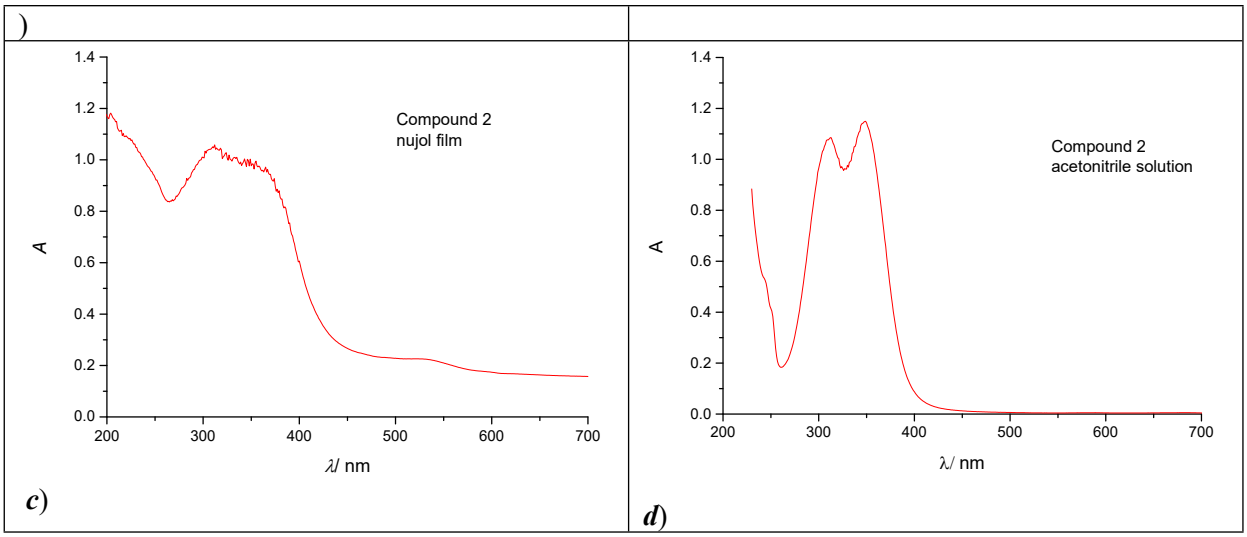

Figure S4 UV-VIS spectra of **1** (*a, b*) and **2** (*c, d*) measured in the nujol suspension (*a*, *c*) and in acetonitrile solution (*b*, *d*).

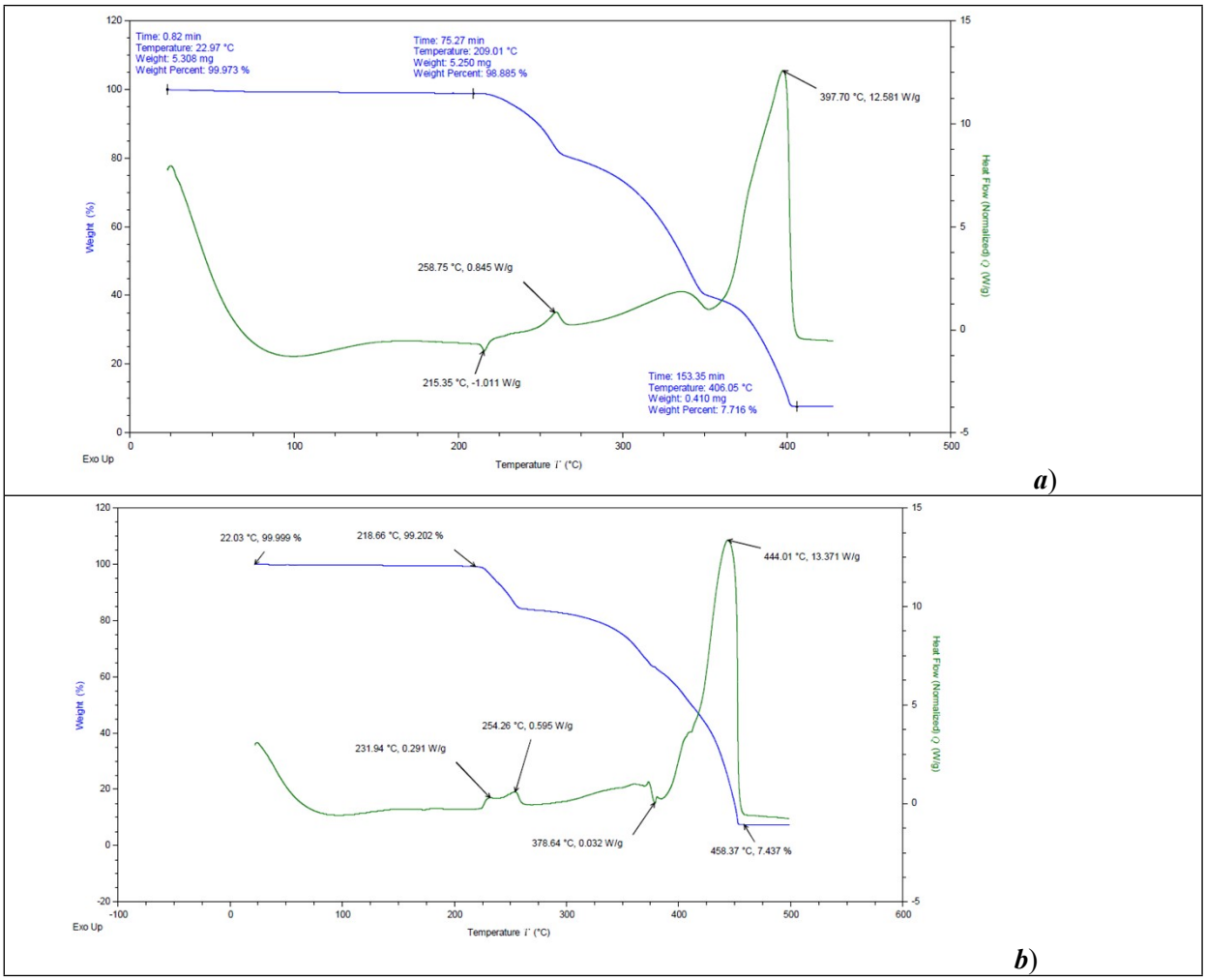

Figure S5 Thermal analysis of **1** (*a*) and **2** (*b*)

S4 Structural information

Table S1 Selected crystallographic information for reported complexes

	1@293K	**1**@100K	**2**@293K	**2**@90K
Formula	$C_{35}H_{45}CoN_7O_6$	$C_{35}H_{45}CoN_7O_6$	$C_{43}H_{61}CoN_7O_6$	$C_{43}H_{61}CoN_7O_6$
M_w / g mol^{-1}	718.71	718.71	830.91	830.91
T / K	293(2)	99.99(11)	293(2)	90.0(2)
λ / Å	1.54184	1.54184	1.54184	1.54184
Crystal system	triclinic	triclinic	triclinic	triclinic
Space group	P -1	P -1	P -1	P -1
a/Å	9.4670(2)	9.3937(2)	9.40245(14)	9.28712(12)
b/Å	14.7604(4)	14.6336(4)	15.00841(17)	14.7721(2)
c/Å	15.1008(4)	14.7677(4)	16.50955(17)	16.32638(15)
α/°	113.491(2)	111.686(2)	96.8096(9)	94.5109(9)
β/°	101.665(2)	102.063(2)	99.3844(11)	100.3059(9)
γ/°	101.979(2)	101.390(2)	101.2737(11)	102.0575(11)
Volume/Å^3	1795.10(8)	1725.84(9)	2226.81(5)	2139.34(5)
Z; ρ_{calc}/g·cm^{-3}	2; 1.320	2; 1.383	2; 1.239	2; 1.290
μ/mm^{-1}	4.190	4.359	3.444	3.584
F(000)	758	758	886	886
GoF	1.035	1.052	1.067	1.038
CCDC no.	2255669	2255671	2255670	2255672

[a] $R1 = \sum(F_0 - F_C)/\sum(F_0)$; $wR2 = \sqrt{\sum[w(F_0^2 - F_C^2)^2]/\sum[w(F_0^2)^2]}$

Table S2 Bond distances and structural parameters of coordination polyhedra calculated for **1** and **2**

	1@293K	**1**@100K	**2**@293K	**2**@90K
Co-N1 / Å	2.100(3)	2.100(2)	2.117(2)	2.103(1)
Co-N2 / Å	2.106(2)	2.095(2)	2.106(2)	2.088(1)
Co-N3 / Å	2.110(3)	2.098(2)	2.103(2)	2.095(1)
Co-O1 / Å	2.037(2)	2.039(2)	2.056(3)/2.03(2)[b]	2.049(1)
Co···O2 / Å	2.970(2)	3.012(2)	2.962(3)/2.68(2)[b]	2.997(1)
Co-O4 / Å	2.108(2)	2.107(2)	2.108(2)	2.103(1)
Co-O5 / Å	2.239(2)	2.219(1)	2.219(2)	2.215(1)
Σ / °	138.5	136.7	137.3	137.4
HP-6[a]	29.307	29.054	28.759/26.978[b]	28.715
PPY-6[a]	19.019	19.452	19.847/19.136 [b]	19.573
OC-6[a]	5.318	4.862	4.858/5.313[b]	4.733
TPR-6[a]	9.602	10.422	10.569/9.305[b]	10.700
JPPY-6[a]	22.495	22.967	23.288/22.197[b]	23.062
COC-7	5.921	5.582	5.407/5.867[b]	5.351
CTPR-7	6.404	6.371	6.305/7.264[b]	6.126

[a]Results of the SHAPE calculations for coordination polyhedra of hexagon (HP-6), pentagonal pyramid (PPY-6), octahedron (OC-6), trigonal prism (TPR-6), Johnson pentagonal pyramid (JPPY-6), Capped octahedron (COC-7), Capped trigonal prism (CTPR-7). [b]for coordination polyhedron involving disordered nitrate oxygen donor atoms O1A and O2A with occupancy factor 0.153(4).

Table S3 Angles of coordination polyhedra for the reported complexes.

angles	**1HT** /º	**2LT** /º	**1HT** /º	**2-LT** /º
O1-Co-O4	99.82(9)	102.72(1)	102.71(12)	102.31(4)
O1-Co-O5	157.64(9)	161.03(12)	161.02(12)	161.74(4)
O1-Co-N1	91.27(9)	99.77(11)	99.80(11)	92.26(4)
O1-Co-N2	87.60(8)	86.29(12)	86.34(12)	84.96(4)
O1-Co-N3	101.62(9)	90.70(10)	90.66(10)	98.56(4)
O4-Co-O5	58.65(8)	59.01(8)	59.01(7)	59.80(4)
O4-Co-N1	105.15(8)	103.39(8)	103.39(7)	102.48(4)
N1-Co-O5	89.13(9)	90.24(7)	90.24(7)	88.60(4)
N2-Co-O4	172.54(8)	170.98(7)	170.94(7)	172.66(4)
N2-Co-O5	114.04(8)	111.98(7)	111.93(7)	112.88(4)
N2-Co-N1	75.21(8)	75.22(7)	75.24(7)	75.99(5)
N3-Co-O4	102.28(9)	103.59(8)	103.60(8)	103.88(4)
N3-Co-O5	89.88(9)	89.16(8)	89.16(7)	90.03(4)
N3-Co-N1	147.12(9)	148.02(7)	148.04(7)	148.55(5)
N3-Co-N2	75.26(8)	75.42(7)	75.40(7)	75.67(5)

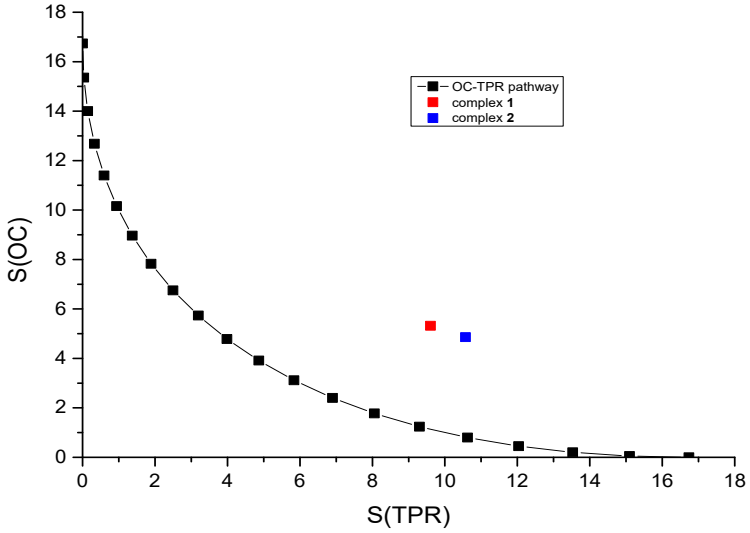

Figure S6 Symmetry measure parameters of reported structures obtained by SHAPE structural analysis and their positions on the continuous shape map representing the Bailar twist between octahedral (OC) and trigonal prismatic geometry (TPR).

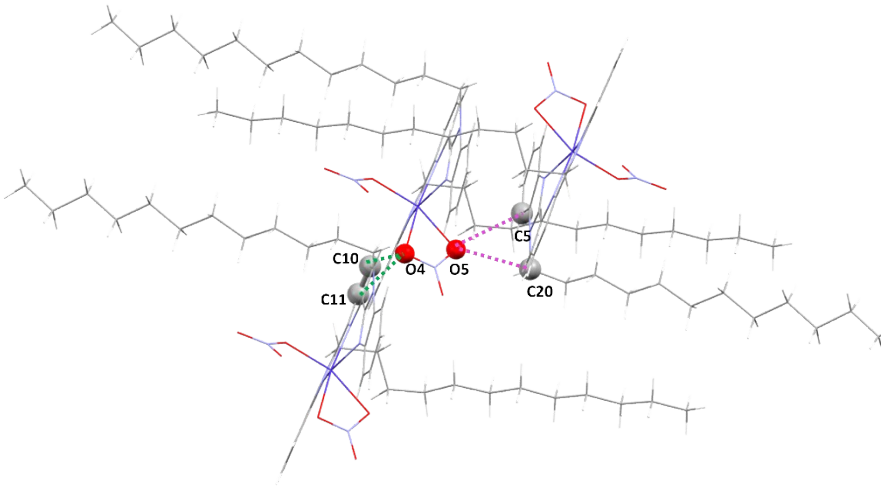

Figure S7 Visualization of intra-dimeric (magenta) and inter-dimeric (green) non-covalent interactions in compound **2**: O5···C5=3.097(2) Å, O5···C20=3.161(2) Å, O4···C10=3.132(2) Å, O4···C11=3.124(2) Å at 90 K; O5···C5=3.206(3) Å, O5···C20=3.210(3) Å, O4···C10=3.259(3) Å, O4···C11=3.263(3) Å at 293 K.

S3 Surface characterisation

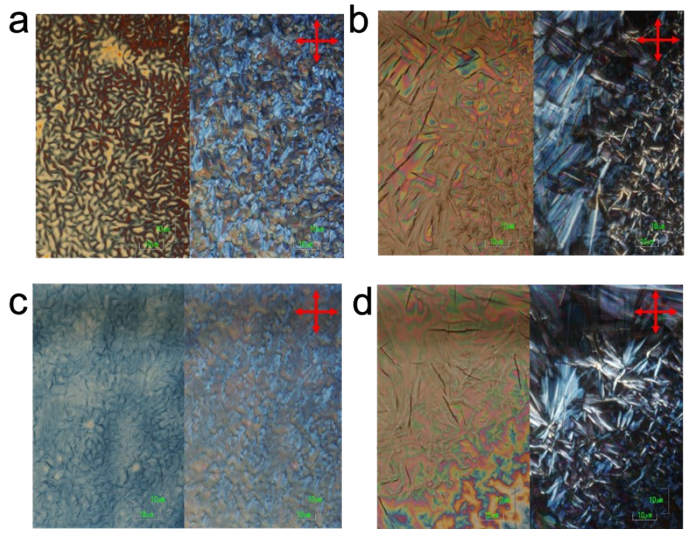

Figure S8 Optical micrographs of drop cast films of **1** and **2** compounds recorded by optical microscopy in bright field (left) and with crossed polars (right). First line refers to compound **1** measured at centre (*a*) of the film and at the boundary (*b*). Second line refers to compound **2** measured at centre (*c*) of the film and at the boundary (*d*).

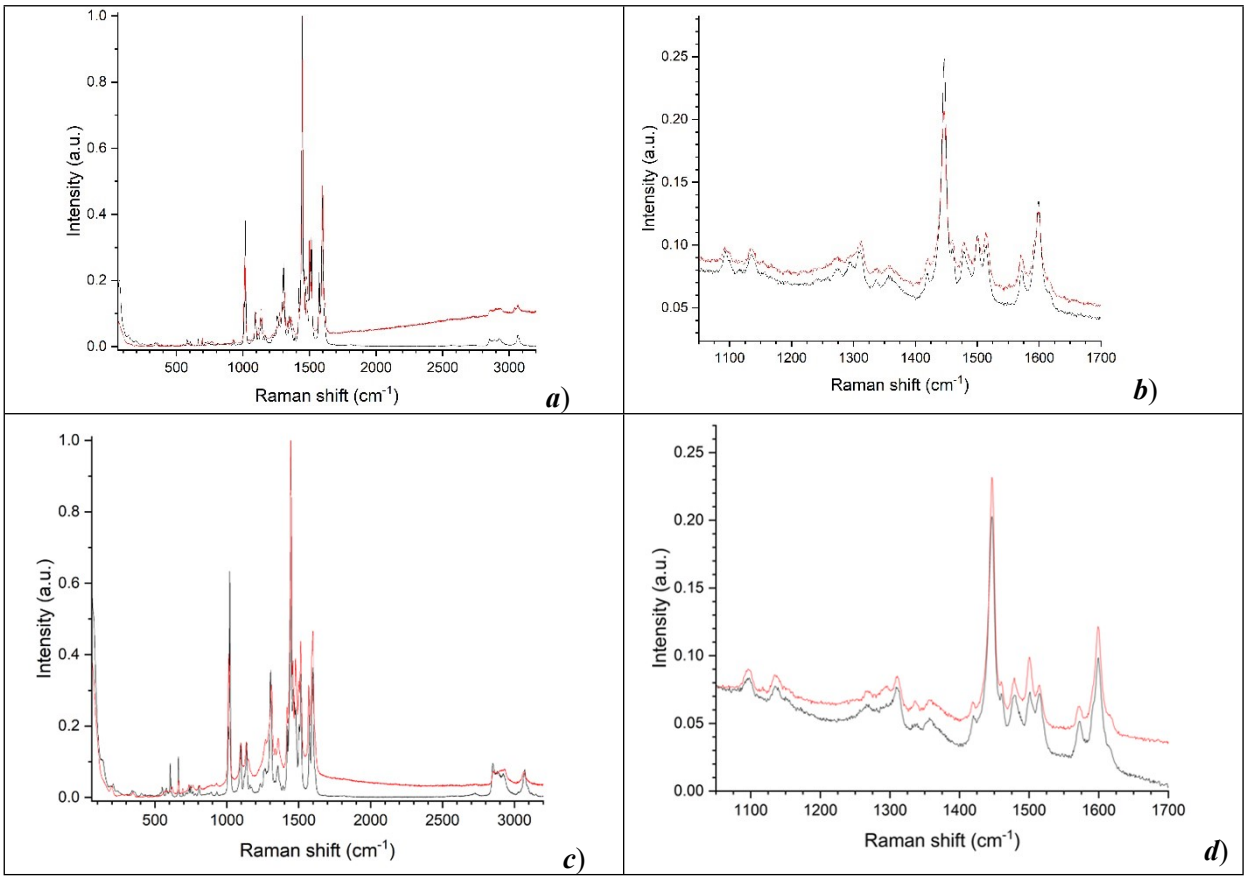

Figure S9 Raman spectroscopy of compound **1** (*a*; powder - black line, drop casted film - red line); (*b*; zoomed spectra of drop casted film - black line, printed structures by lithographically controlled wetting - red line). Raman spectroscopy of compound **2** (***c***; powder - black line, drop casted film - red line); (*d*

- zoomed Raman spectra of drop casted film - black line; printed structures by lithographically controlled wetting - red line).

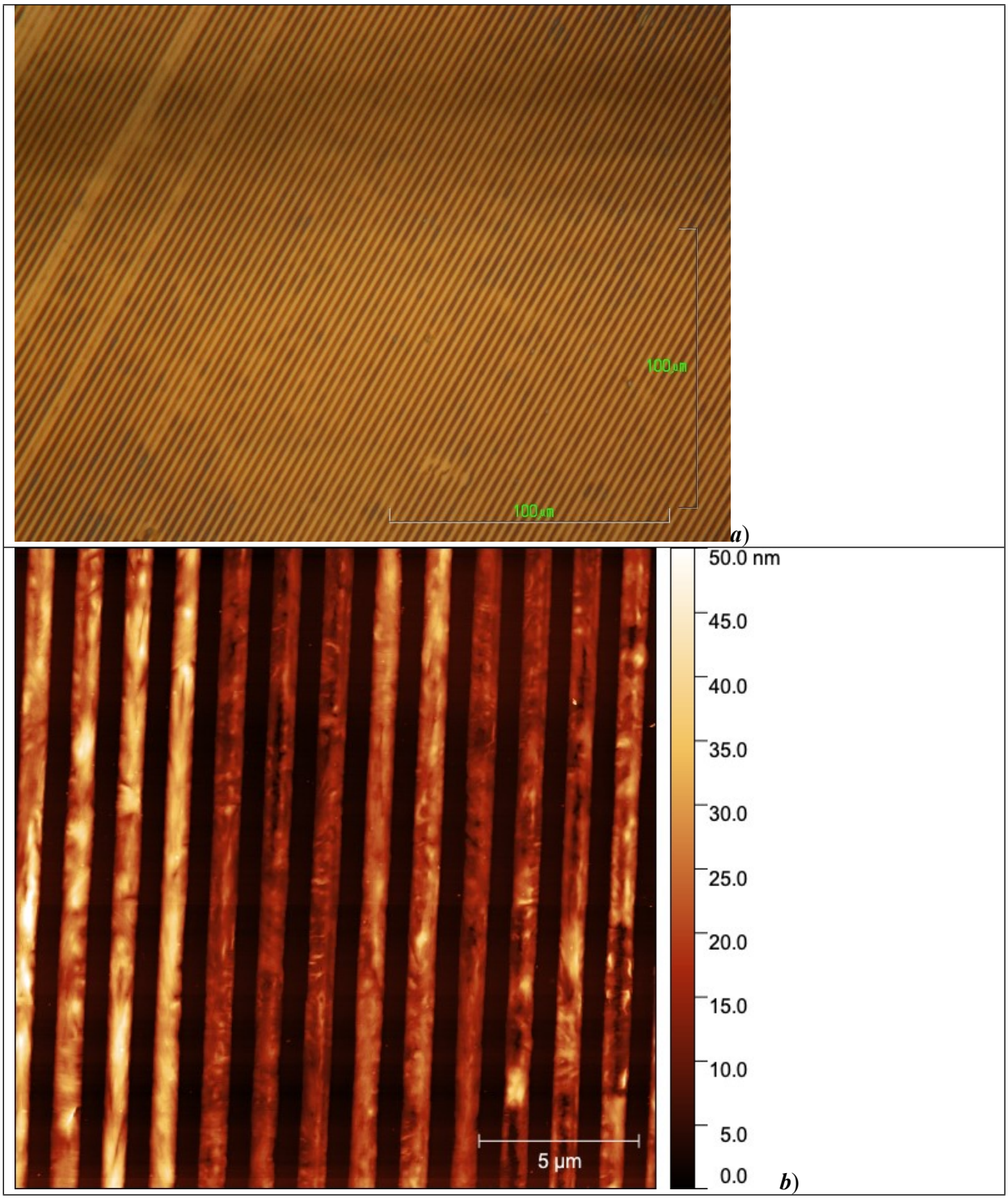

Figure S10 Printed structures of **2** fabricated by lithographically controlled wetting on silicon surface *(a)*; AFM morphology of printed stripes, bar is 5 µm, *z* scale 0-50 nm **(***b*).

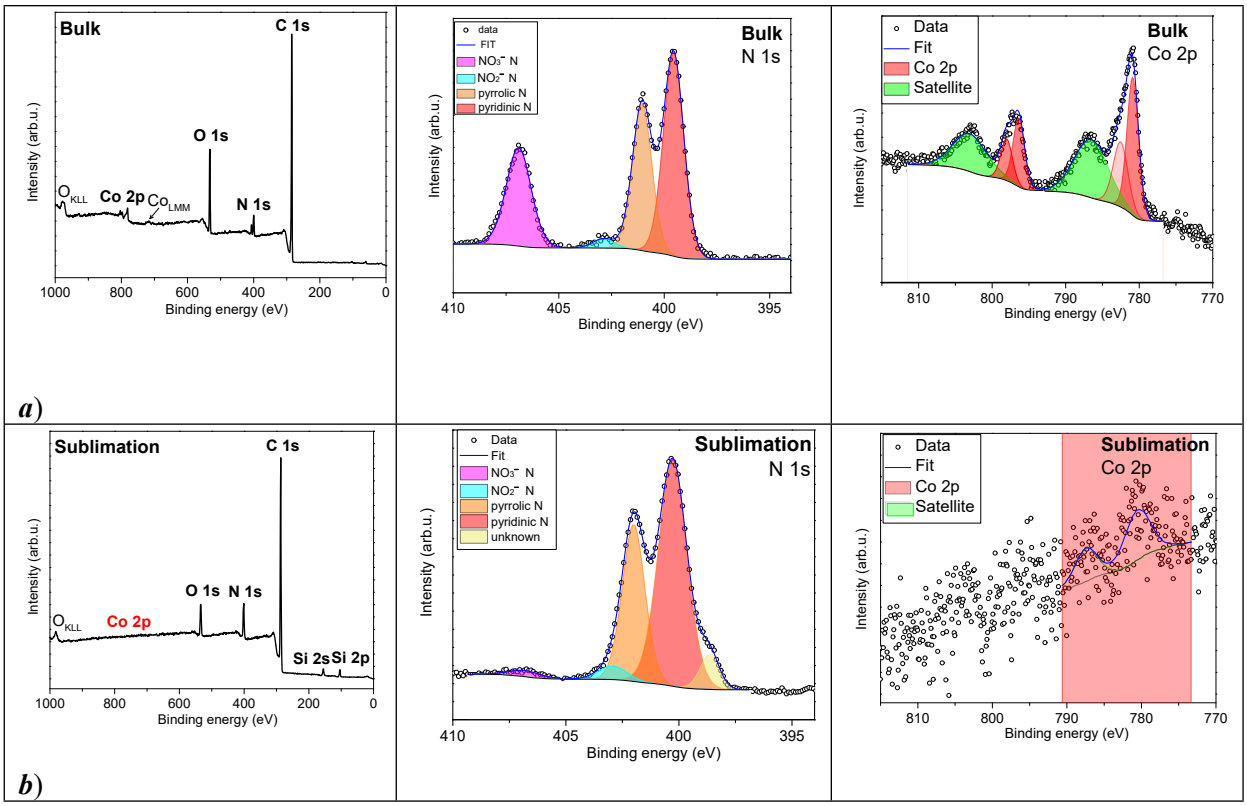

Figure S11 XPS for the compound **1** in the bulk (*a*) and after sublimation on graphene surface (*b*).

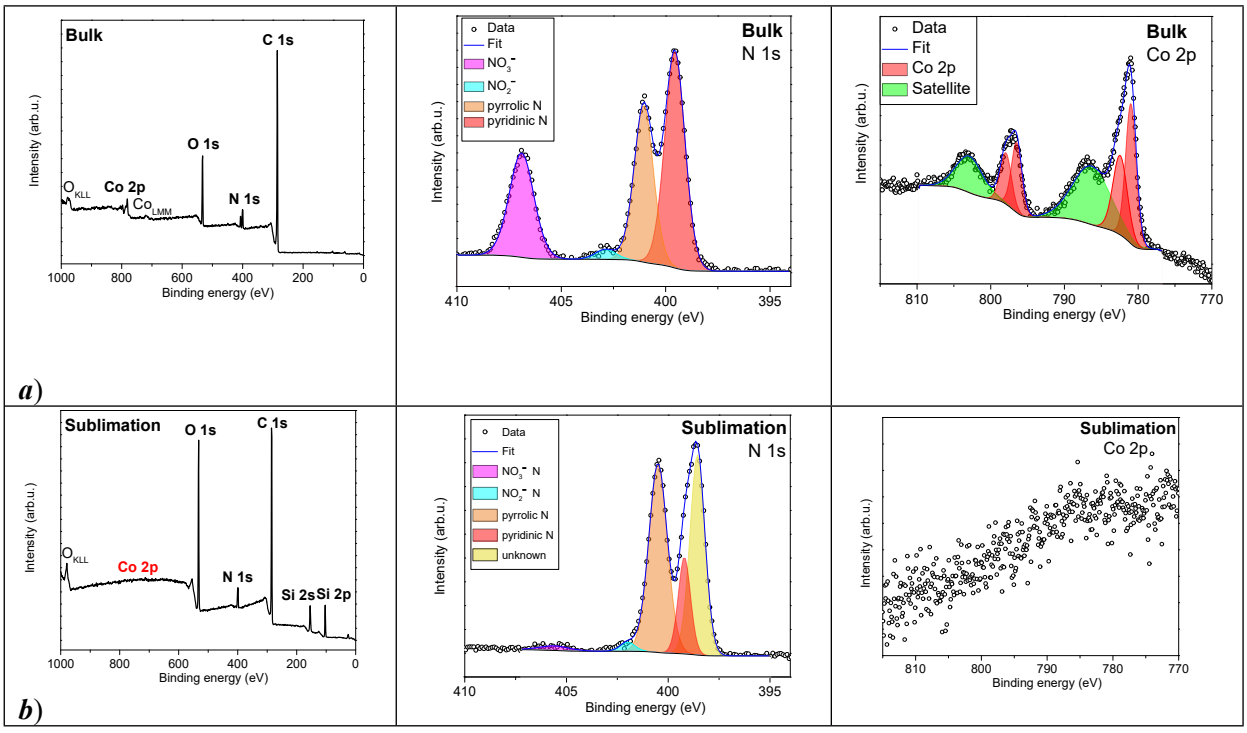

Figure S12 XPS for the compound **2** in the bulk (*a*) and after sublimation on graphene surface (*b*).

S5 Computational Study and Static Magnetic Properties

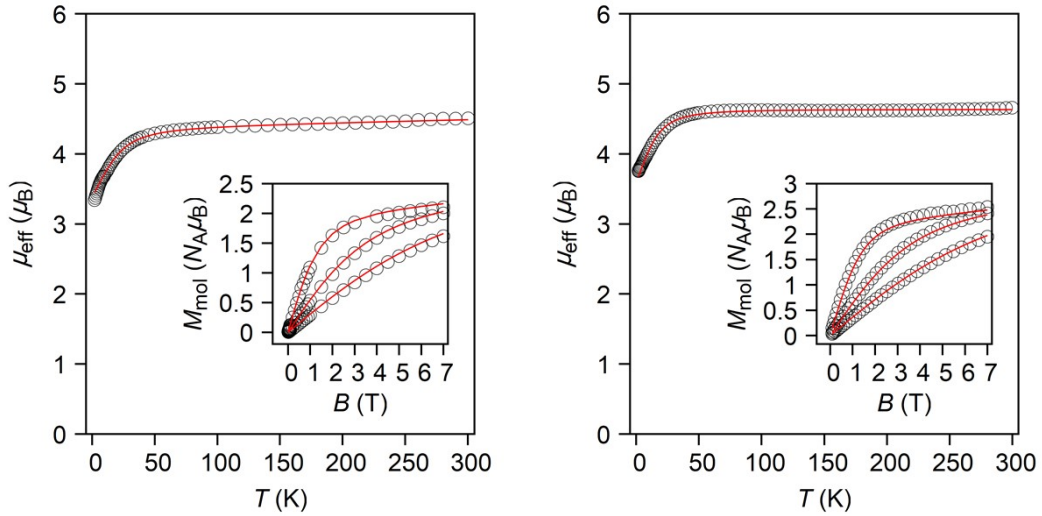

Figure S13 Temperature dependence of the effective magnetic moment and isothermal magnetizations measured at $T = 2$, 5 and 10 K (shown in the inset) for **1** (*left*) and **2** (*right*). Empty symbols – experimental data, full lines – calculated data with $D = +19.5$ cm^{-1}, $E = +6.4$ cm^{-1}, $g_{iso} = 2.253$, $\chi_{TIP} = 5.8\times10^{-9}$ mol m^{-3} for **1**, and $D = +17.06$ cm^{-1}, $E = 0$ cm^{-1}, $g_{iso} = 2.3920$ for **2**.

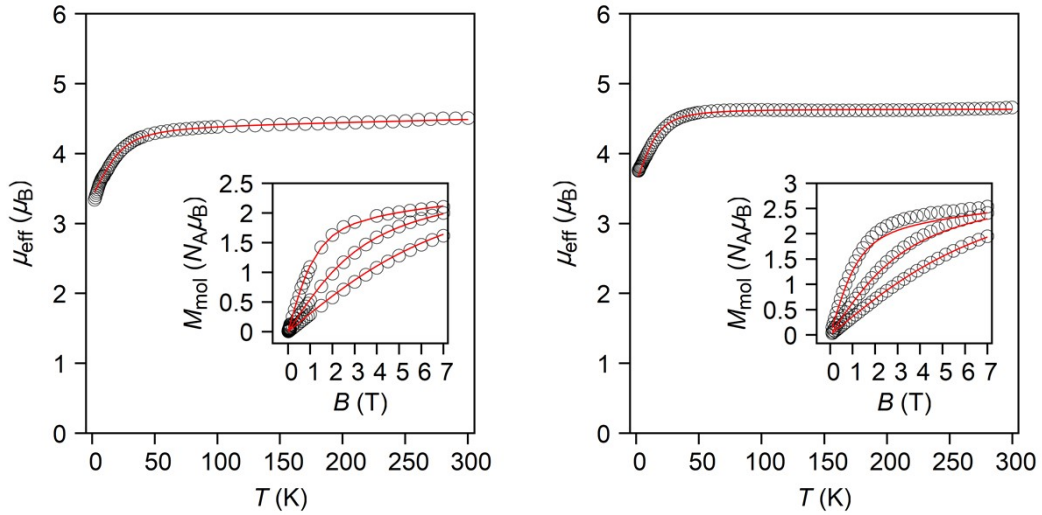

Figure S14 Temperature dependence of the effective magnetic moment and isothermal magnetizations measured at $T = 2$, 5 and 10 K (shown in the inset) for **1** (*left*) and **2** (*right*). Empty symbols – experimental data, full lines – calculated data with $D = -20.6$ cm^{-1}, $E = -5.0$ cm^{-1}, $g_{iso} = 2.254$, $\chi_{TIP} = 5.7\times10^{-9}$ mol m^{-3} for **1**, and $D = -14.46$ cm^{-1}, $E = -4.77$ cm^{-1}, $g_{iso} = 2.3919$ for **2**.

S6 HF EPR and FIRMS spectroscopy

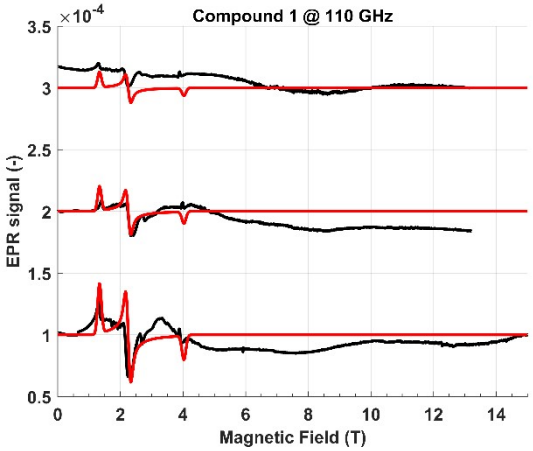

Figure S15 Temperature dependence of the HFEPR spectra (black) of complex **1** at 5 K, 12 K and 20 K (from bottom to top respectively). Red lines are simulations using parameters from table 3 (see main text).

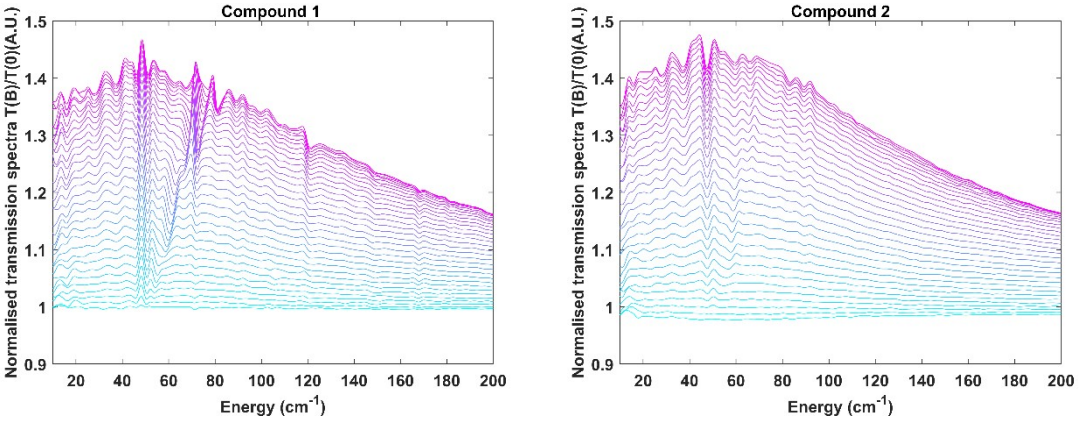

Figure S16 FIRMS spectra of complexes **1** and **2** normalised by the reference at zero magnetic field. The field-dependent peaks are not evident in this visualization compared to the normalisation by the adjacent spectrum and differentiation, shown as a contour plot in the main text.

S7 X-band EPR spectroscopy

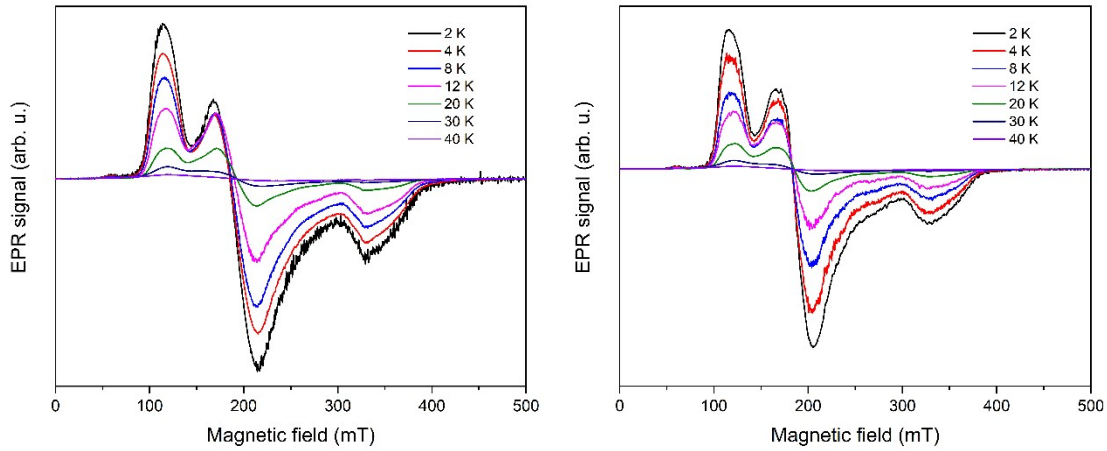

Figure S17 Temperature evolution of the X-band EPR spectra of complex **1** (left) and **2** (right).

S8 Dynamic magnetic investigation

The magnetic data induced by the oscillating; alternating-current (AC) magnetic field were obtained at an amplitude of B_{AC} = 0.38 mT. To determine the optimum DC field to suppress the quantum tunnelling of magnetization, AC susceptibility measurements under various DC fields were applied at 2 K (Figure S14). Collected sets of χ' and χ'' (susceptibilities (18 χ' and 18 χ'') at each DC field were fitted using the formulas for extended one-set Debye model

$$\chi'(\omega) = \chi_S + (\chi_T - \chi_S)\frac{1+(\omega\tau)^{(1-\alpha)}\sin(\pi\alpha/2)}{1+2(\omega\tau)^{(1-\alpha)}\sin(\pi\alpha/2)+(\omega\tau)^{(2-2\alpha)}} \quad \textbf{(S1)}$$

$$\chi''(\omega) = (\chi_T - \chi_S)\frac{(\omega\tau)^{(1-\alpha)}\cos(\pi\alpha/2)}{1+2(\omega\tau)^{(1-\alpha)}\sin(\pi\alpha/2)+(\omega\tau)^{(2-2\alpha)}} \quad \textbf{(S2)}$$

or two-set Debye model (high-field measurements **1** and **2** at 2 K, see Tables S5 and S7)

$$\chi'(\omega) = \chi_S + (\chi_{T1} - \chi_S)\frac{1+(\omega\tau_1)^{(1-\alpha_1)}\sin(\pi\alpha_1/2)}{1+2(\omega\tau_1)^{(1-\alpha_1)}\sin(\pi\alpha_1/2)+(\omega\tau_1)^{(2-2\alpha_1)}} + (\chi_{T2} - \chi_{T1})\frac{1+(\omega\tau_2)^{(1-\alpha_2)}\sin(\pi\alpha_2/2)}{1+2(\omega\tau_2)^{(1-\alpha_2)}\sin(\pi\alpha_2/2)+(\omega\tau_2)^{(2-2\alpha_2)}} \quad \textbf{(S3)}$$

$$\chi''(\omega) = (\chi_{T1} - \chi_S)\frac{(\omega\tau_1)^{(1-\alpha_1)}\cos(\pi\alpha_1/2)}{1+2(\omega\tau_1)^{(1-\alpha_1)}\sin(\pi\alpha_1/2)+(\omega\tau_1)^{(2-2\alpha_1)}} + (\chi_{T2} - \chi_{T1})\frac{(\omega\tau_2)^{(1-\alpha_2)}\cos(\pi\alpha_2/2)}{1+2(\omega\tau_2)^{(1-\alpha_2)}\sin(\pi\alpha_2/2)+(\omega\tau_2)^{(2-2\alpha_2)}} \quad \textbf{(S4)}$$

The optimal DC field for the temperature dependent AC susceptibility investigation has been determined at the maximum of the τ vs B curve and it was 0.15 T for **1** and 0.07 T for **2**. Temperature dependent dynamic magnetic investigation has been measured in the temperature range 2-5.2 K and collected sets of χ' and χ'' (susceptibilities (14 χ' and 14 χ'') at each DC field were fitted using the formulas for extended one-set Debye model (eq. S1 and S2).

Table S4 Conditions of AC magnetic experiments for compound **1**.

	B_{DC} / T	B_{AC} / mT	T / K	Frequency range
1	0 – 1 T (18 steps)	3.5	2 K	0.1 Hz -1488.1 Hz (28 steps)
	0.15 T	3.5	2.0-5.2 K (14 steps)	0.1 Hz -1488.1 Hz (36 steps)
2	0 – 1 T (18 steps)	3.5	2 K	0.1 Hz -1488.1 Hz (28 steps)
	0.07 T	3.5	2.0-5.2 K (14 steps)	0.1 Hz -1488.1 Hz (36 steps)

Table S5 Parameters of the extended one-set Debye model (eq. S1 and S2) for **1** measured from 0 T to 1 T at T = 2.0 K.

B / T	χ_T /10^{-6} cm^3 mol^{-1}	χ_S /10^{-6} cm^3 mol^{-1}	α /10^{-2}	τ /10^{-3} s	R^2
0.005	9.76(2)	0.03(2)	28.0(3)	7.61(5)	0.9998
0.01	10.141(6)	7.016(9)	26.5(4)	2.28(9)	0.9999
0.02	10.201(8)	3.840(11)	27.9(2)	3.27(2)	0.9997
0.03	10.22(1)	2.29(1)	28.3(2)	4.14(2)	0.9996
0.04	10.22(1)	1.50(1)	28.6(2)	4.77(2)	0.9999
0.05	10.20(1)	1.08(1)	28.6(2)	5.33(3)	0.9999
0.06	10.19(2)	0.83(1)	28.6(3)	5.84(3)	0.9989
0.07	10.19(2)	0.67(1)	28.6(3)	6.33(4)	0.9999
0.08	10.19(2)	0.56(2)	28.6(3)	6.81(5)	0.9998

0.09	10.19(2)	0.48(2)	28.7(3)	7.26(5)	0.9998
0.1	10.18(2)	0.43(2)	28.6(3)	7.67(5)	0.9998
0.125	10.15(2)	0.35(2)	28.1(3)	8.53(6)	0.9998
0.15	10.08(2)	0.32(2)	27.2(3)	9.06(6)	0.9998
0.2	9.80(2)	0.28(2)	25.4(3)	8.95(6)	0.9998
0.3	9.00(5)	0.13(4)	27.5(7)	6.48(1)	0.9990
0.4 LF	6.70(6)	0	45.2(7)	9.79(5)	0.9996
0.4 HF	8.48(5)		01.0(5)	1.41(5)	
0.5 LF	6.2(1)	0.07(6)	50(1)	13.12(9)	0.9997
0.5 HF	7.96(8)		0	0.7(2)	

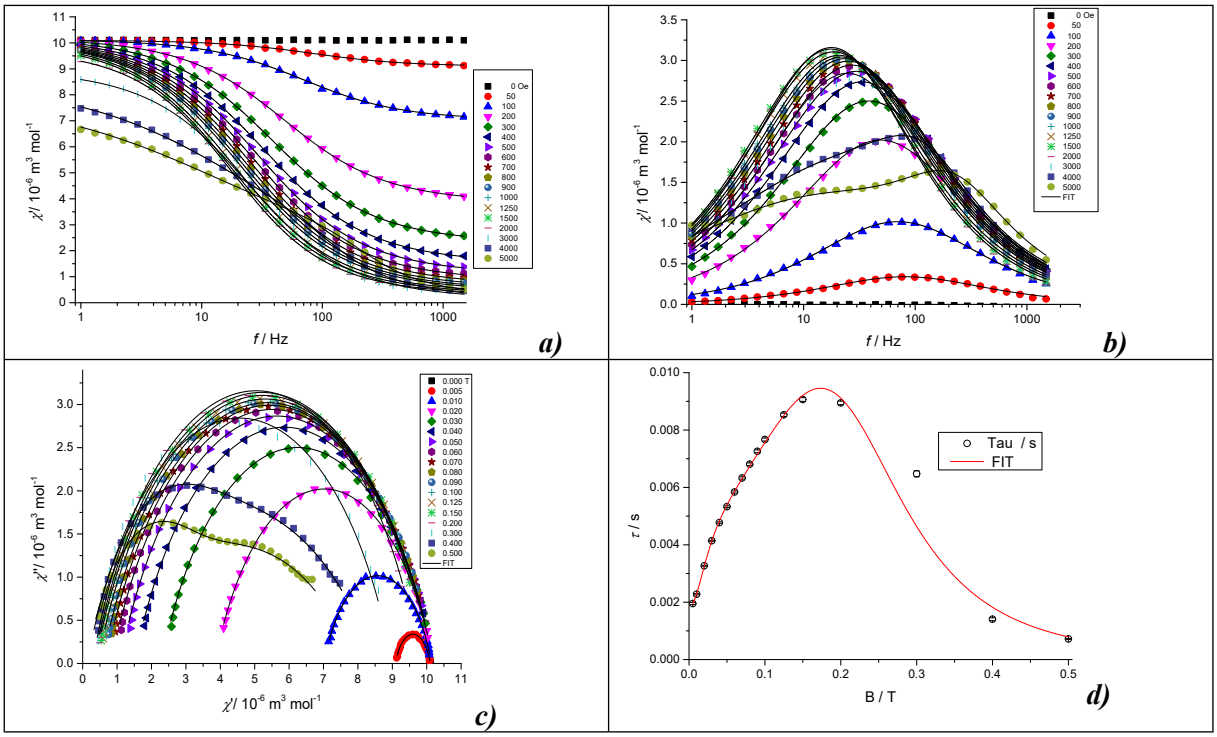

Figure S18 AC susceptibility data for **1** recorded at various static magnetic fields at T = 2.0 K: Frequency dependent in-phase χ'(a) and out-of-phase χ''(b) component of AC susceptibility and Cole-Cole diagram (c) (solid lines are results of fits according to equations S1 and S2). Field dependency of relaxation time τ (with standard errors) fitted to equation (2) (see main text).

Table S6 Parameters of the extended one-set Debye model (eq. S1 and S2) for **2** measured from 0 T to 1 T at T = 2.0 K.

B / T	χ_T /10^{-6} cm^3 mol^{-1}	χ_S /10^{-6} cm^3 mol^{-1}	α /10^{-2}	τ /10^{-3} s	R^2
0.005	10.502(2)	9.473(9)	6.2(6)	0.21(3)	0.9999
0.01	10.51(2)	7.33(1)	6.20(3)	0.27(2)	0.9999
0.02	10.52(8)	4.02(2)	8.13(2)	0.42(2)	0.9998
0.03	10.52(1)	2.43(2)	9.07(2)	0.57(2)	0.9996
0.04	10.51(1)	1.63(2)	9.54(2)	0.67(3)	0.9999
0.05	10.50(1)	1.20(2)	9.76(2)	0.73(3)	0.9999
0.06	10.47(2)	0.95(2)	9.99(2)	0.75(3)	0.9999

0.07	10.44(7)	0.76(1)	10.52(2)	0.76(2)	0.9999
0.08	10.41(5)	0.62(2)	11.01(1)	0.74(2)	0.9999
0.09	10.38(2)	0.53(1)	11.57(1)	0.72(2)	0.9998
0.1	10.33(2)	0.44(1)	12.3(1)	0.69(2)	0.9999
0.125	10.21(1)	0.25(2)	14.5(3)	0.60(3)	0.9998
0.15	10.06(1)	0.06(5)	17.3(4)	0.51(5)	0.9998
0.2	9.70(3)	0	22.8(7)	0.37(6)	0.9989
0.3 LF	2.93(3)	0	55(4)	24(3)	0.9999
0.3 HF	10.1(1)		22.5(8)	0.15(2)	
0.4 LF	4.2(2)	0	55.4(2)	35(1)	0.9999
0.4 HF	9.78(8)		28.0(8)	0.065(8)	
0.5 LF	4.8(2)	0	55(1)	56.9(3)	0.9999
0.5 HF	9.4(1)		35.7(1)	0.7(2)	

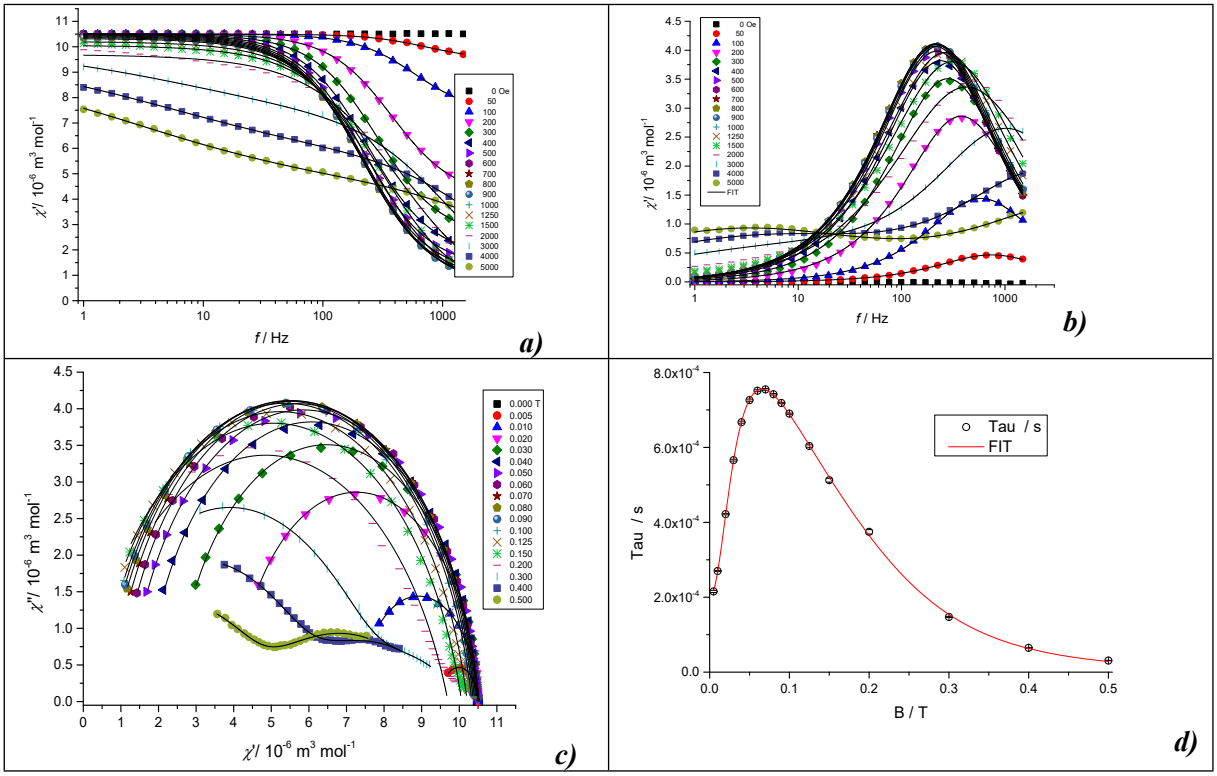

Figure S19 AC susceptibility data for **2** recorded at various static magnetic fields at T = 2.0 K: Frequency dependent in-phase χ'(*a*) and out-of-phase χ''(*b*) component of AC susceptibility and Cole-Cole diagram (*c*) (solid lines are results of fits according to equations S1 and S2). (*d*) Field dependency of relaxation time τ (with standard errors) fitted to equation (2) (see main text).

Table S7 Relaxation parameters at T = 2 K for compounds **1** and **2** obtained from fits using the combinations of quantum tunnelling (QTM), Raman and direct processes according to equation (2) (see main text).

	Compound 1	**Compound 2**
QTM	b_1 = 380.37 ± 45.92 s^{-1} b_2 = 4121.38 ±1345.39 T^{-2}	b_1 = 4080.29 ± 101.96 s^{-1} b_2 = 4643.35 ± 284.87 T^{-2}
Raman	d = 0.33 ± 0.03 s^{-1} K^{-9} e = 9.70 ± 14.01 T^{-2}	d = 1.83 ± 0.05 s^{-1} K^{-9} e = 75.39 ±15.01 T^{-2}

	$f = 51.29 \pm 32.25$ T^{-2} $n = 9$ (fixed)	$f = 24.86 \pm 7.58$ T^{-2} $n = 9$ (fixed)
direct	$A = (9792.31 \pm 1218.97)$ s^{-1} T^{-4} K^{-1} $m = 4$ (fixed)	$A = (260833.83 \pm 16353.6)$ s^{-1} T^{-4} K^{-1} $m = 4$ (fixed)
R^2	0.9927	0.9997

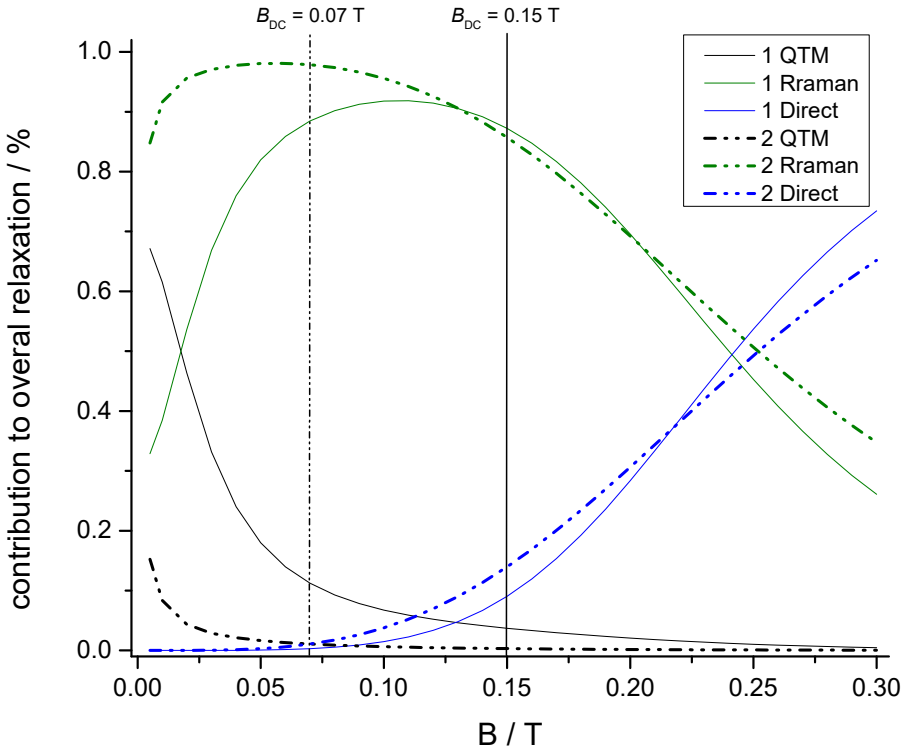

Figure S20 The individual contributions of relaxation processes to the overall relaxation at 2 K. Simulations were calculated from relaxation parameters listed in Table S7.

Table S8 Parameters of the extended one-set Debye model (eq. S1 and S2) for **1** measured at 0.15 T.

T /K	χ_T /10^{-6} cm^3 mol^{-1}	χ_S /10^{-6} cm^3 mol^{-1}	α /10^{-2}	τ /10^{-3} s	R^2
2.0	9.76(2)	0.30(2)	28.1(3)	7.61(5)	0.9998
2.2	8.95(2)	0.28(2)	28.9(3)	5.88(4)	0.9998
2.4	8.34(2)	0.28(1)	28.8(3)	4.63(3)	0.9998
2.6	7.73(1)	0.28(1)	28.4(3)	3.53(2)	0.9999
2.8	7.22(1)	0.30(1)	27.3(3)	2.69(2)	0.9999
3.0	6.76(1)	0.33(2)	25.9(3)	2.04(1)	0.9998
3.2	6.37(1)	0.37(2)	23.6(3)	1.54(1)	0.9998
3.4	6.00(1)	0.42(2)	20.8(4)	1.14(1)	0.9997
3.6	5.68(1)	0.47(2)	17.1(4)	0.82(8)	0.9997
3.8	5.39(7)	0.52(2)	13.1(4)	0.57(5)	0.9998
4.0	5.13(5)	0.54(2)	9.36(3)	0.37(2)	0.9998
4.4	4.71(2)	0.54(2)	3.81(3)	0.15(9)	0.9998
4.8	4.36(2)	0.4(1)	2.8(6)	0.05(2)	0.9999
5.2	4.07(2)	0	3.24(5)	0.0164(2)	0.9999

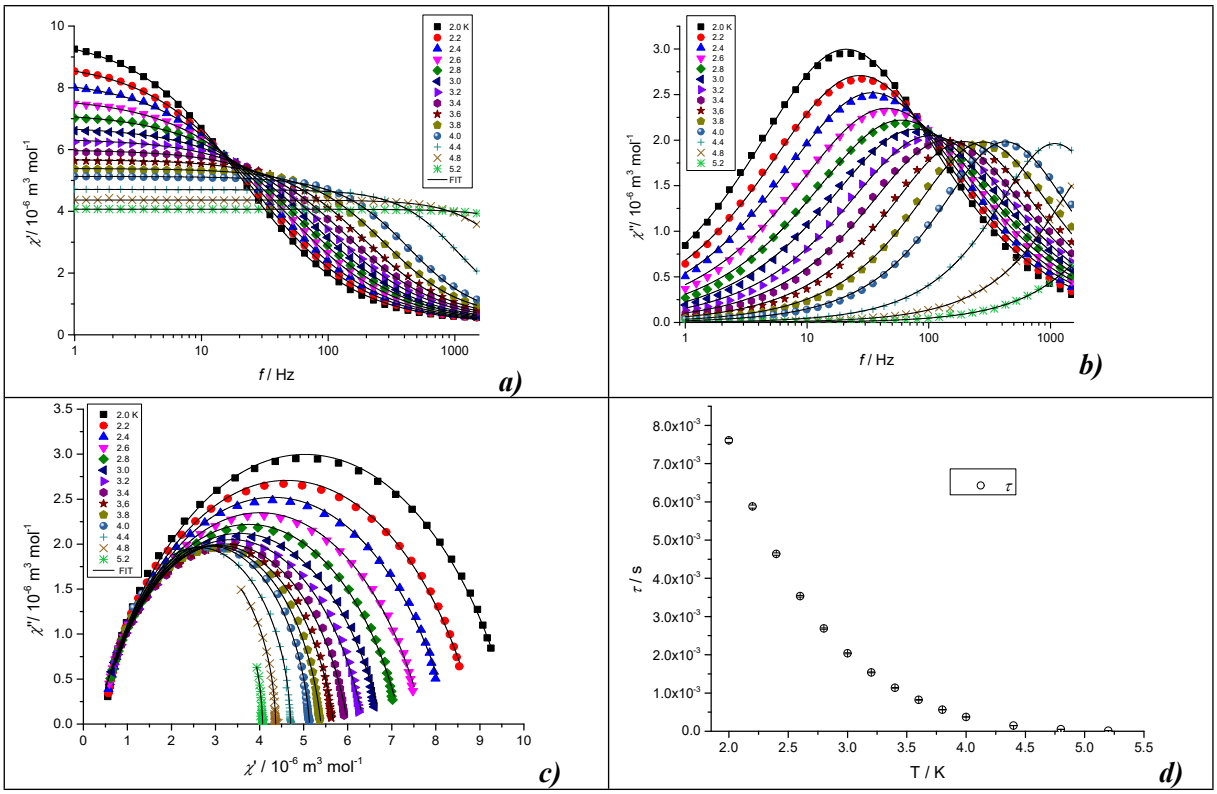

Figure S21 AC susceptibility data for **1** recorded in temperature range 2-5,2 K: Frequency dependent in-phase χ'(*a*) and out-of-phase χ''(*b*) component of AC susceptibility and Cole-Cole diagram (*c*) (solid lines are results of fits according to equations S1 and S2). (*d*) Temperature dependency of relaxation time τ (with standard errors).

Table S9 Parameters of the extended one-set Debye model (eq. S1 and S2) for **2** measured at 0.07 T.

T /K	χ_T /10^{-6} cm^3 mol^{-1}	χ_S /10^{-6} cm^3 mol^{-1}	α /10^{-2}	τ /10^{-3} s	R^2
2.0	10.45(5)	0.73(1)	10.5(1)	0.77(2)	0.9999
2.2	9.55(6)	0.71(2)	10.4(3)	0.62(2)	0.9999
2.4	8.88(5)	0.68(2)	10.4(2)	0.52(2)	0.9998
2.6	8.25(6)	0.68(1)	10.2(2)	0.43(2)	0.9999
2.8	7.70(5)	0.69(2)	9.95(2)	0.36(2)	0.9999
3.0	7.23(6)	0.70(3)	9.62(3)	0.31(2)	0.9999
3.2	6.82(6)	0.71(3)	9.35(3)	0.27(1)	0.9999
3.4	6.45(6)	0.09(4)	8.6(4)	0.23(2)	0.9999
3.6	6.12(5)	0.80(3)	7.8(4)	0.19(2)	0.9999
3.8	5.83(7)	0.86(3)	6.2(4)	0.16(2)	0.9999
4.0	5.56(5)	0.89(2)	4.55(3)	0.13(1)	0.9999
4.4	5.10(1)	0.89(2)	1.44(6)	0.068(6)	0.9998
4.8	4.73(2)	0.3(4)	2.5(1)	0.026(3)	0.9999
5.2	4.40(2)	0	0.89(6)	0.010(2)	0.9999

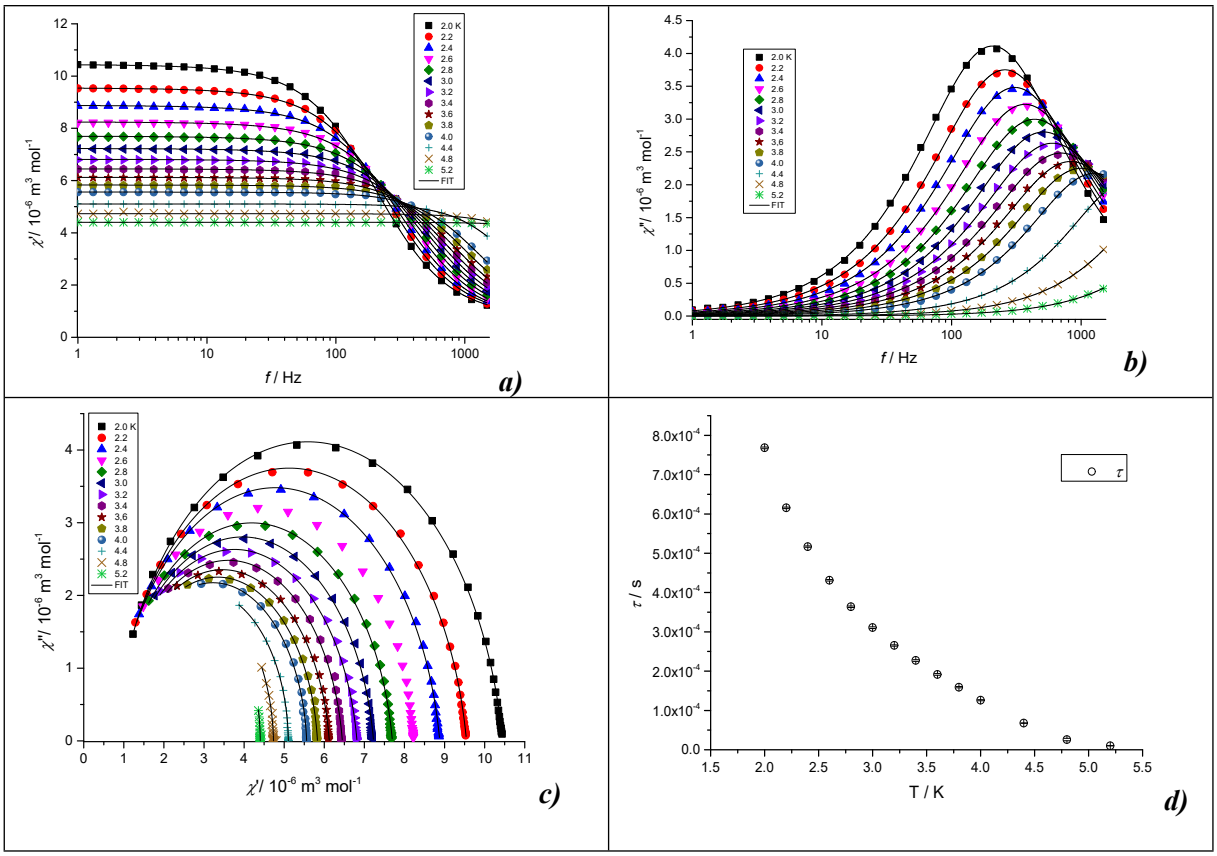

Figure S22 AC susceptibility data for **2** recorded in temperature range 2-5.2 K: Frequency dependent in-phase χ'(*a*) and out-of-phase χ''(*b*) component of AC susceptibility and Cole-Cole diagram (*c*) (solid lines are results of fits according to equations S1 and S2). (*d*) Temperature dependency of relaxation time τ (with standard errors).

Table S10 Relaxation parameters at B_{DC} = 0.15 T for compound **1** using the respective combinations of Orbach. Raman and Direct processes of relaxation.

	U/k_B / K	τ_0/s	C / K^{-n} s^{-1}; n	A / s^{-1} T^{-4} K^{-1} m = 4 (fixed)	R^2
Compound 1 @ 0.15 T					
Orbach[a]	62(4)	1.0(9)×10^{-10}	-	-	0.99282
Orbach & Raman & direct	77(4)	7(2)x10^{-12}	0.6(1) 5.8(2)	1.00(4)x10^{5}	0.9999
Compound 2 @ 0.07 T					
Orbach[a]	54(2)	3(1)×10^{-10}	-	-	0.99747
Orbach & Raman	70(2)	1.6(5)×10^{-11}	264(9) 2.28(3)	-	0.99977

[a]for data in the range 4.4 K–5.2 K

References

[1] J. Juráková, J. Dubnická Midlíková, J. Hrubý, A. Kliuikov, V. T. Santana, J. Pavlik, J. Moncoľ, E. Čižmár, M. Orlita, I. Mohelský, P. Neugebauer, D. Gentili, M. Cavallini, I. Šalitroš., *Inorg. Chem. Front.*, 2022, **9**, 1179.

[2] M. Cavallini, D. Gentili, P. Greco, F. Valle, F. Biscarini, *Nature Protocols*, 2012, 7, 1668-1676.

[3] D. A. Shirley, "High-resolution X-ray photoemission spectrum of the valence bands of gold," Phys. Rev. B, 1972, **5**, 4709–4714.

[4] Rigaku Oxford Diffraction (2020) CrysAlisPro 1.171.40.82a.

[5] G. M. Sheldrick, *Acta Crystallogr. Sect.* 2015, *A* 71, 3–8.

[6] L. J. Bourhis, O. V. Dolomanov, R. J. Gildea, J. A. K. Howard, H. Puschmann, *Acta Crystallogr. Sect. A 71* (2015) 59–75, doi:10.1107/S2053273314022207.

[7] O. V. Dolomanov, L. J. Bourhis, R. J. Gildea, J. A. K. Howard, H. Puschmann, *J. Appl. Crystallogr.* 42 (2009) 339–341.

[8] R. Boča. Theoretical Foundations of Molecular Magnetism. Elsevier. Amsterdam. 1999.

[9] a) A. Sojka, M. Šedivý, O. Laguta, A. Marko, V. T. Santana, P. Neugebauer. High-frequency EPR: current state and perspectives. *Electron Paramagnetic Resonance* 2020. DOI: 10.1039/9781839162534-00214. b) A. Sojka, M. Šedivý, A. Lagiň, A. Gabriš, T. Láznička, V. T. Santana, O. Laguta, P. Neugebauer. IEEE Transactions on instrumentation and measurement 2022, **71**, 8002812. DOI: 10.1109/TIM.2022.3164135.

[10] a) S. Stoll, A. Schweiger. J. Magn. Reson. 2006, **178**, 42-55. DOI: 10.1016/j.jmr.2005.08.013 b) J. Nehrkom, J. Telser, K. Holldak, S. Stoll, A. Schnegg. *J. Phys. Chem. B* 2015, **119**, 13816–13824. DOI: 10.1021/acs.jpcb.5b04156

[11] MATLAB version: 9.13.0 (R2022b), Natick, Massachusetts: The MathWorks Inc.; 2022.